Influence of Inverter-interfaced Renewable Energy Generators on Directional Relay and an Improved Scheme

Ke Jia, *Member, IEEE*, Zhe Yang, Yu Fang, Tianshu Bi, *Senior Member, IEEE* and Mark Sumner, *Senior Member, IEEE*

***Abstract*—Renewable energy sources (RESs) are typically interfaced to the grid using power electronics which can cause their fault current characteristics to display significant low frequency harmonics and unbalanced sequence impedances. Such current characteristics can lead to the operation failure of fault component based directional relays. To demonstrate the influence of inverter-interfaced renewable energy generators (IIREGs) on directional relays in detail, analytical expressions for the IIREG equivalent positive- and negative-sequence superimposed impedances are derived in this paper. Considering various factors, the angular characteristics of the sequence superimposed impedances are investigated. Based on these attributes, it can be concluded that fault component based directional relays may be unable to operate in some circumstances. A novel high-frequency impedance-based protection scheme is proposed to manage the adaptability problem by determining the fault direction due to a stable impedance angle. The theoretical analysis and the proposed scheme are tested and verified through real time digital simulation (RTDS) simulation and field testing data.**

***Index Terms*—Angular characteristics, directional relay, high-frequency impedance, renewable power sources, sequence superimposed impedance**

I. Introduction

Renewable energy sources (RESs) such as wind power and photovoltaic (PV) power have experienced rapid development in recent years in an attempt to reduce reliance on fossil fuels and associated pollution [1-2]. Such power is now present at all levels of power transmission and distribution systems. As regions rich in wind and solar energy are often located far from the load center, large-scale renewable energy is often sent out through transmission lines [3]. Most RESs are connected to the grid through power electronic inverters, and an LCL filter is installed at the output of the inverter [4-5]. To maintain the security and stability of the power grid, most countries require that wind turbines or PV have certain fault ride-through (FRT) capabilities [6-7], and reactive power is required to support the grid voltage during a fault. A positive- and negative-sequence based control system is often adopted for these purposes and can be controlled in a variety of ways [8-9]. However, different control strategies used by different inverter manufacturers during FRT cause the fault current characteristics of RESs to become unpredictable [10-12], which can impair the correct operation of existing protections [13-14].

At present, the impact analysis of RESs on protection is mainly focused on distance protection and pilot protection. Distance protection has been investigated in [15-18], while literature [15-16] studied the impact of the non-power frequency fault current from doubly fed induction generator (DFIG) based wind farms on distance protection and proposed solutions. In addition, it was determined in [17] that the weak feed of inverter-interfaced renewable energy generators (IIREGs) could amplify the influence of the fault resistance and a corresponding solution was proposed in [18]. However, in this study, a communication system was required for phase faults. For pilot protection, [19] analyzed the reliability and sensitivity of traditional two-terminal differential protection and proposed a novel virtual multi-terminal current differential protection scheme. In [20], after analyzing the reason for sensitivity decline or failure in operation of differential protection for phase faults, a pilot protection based on a correlation coefficient index was proposed to identify faults within a short data window.

A few studies have examined the impact of RESs on the directional relays which are indispensable for lines with double-ended fault currents. In the distribution network, the integration of distributed generation (DG) means that directional overcurrent relays (DORs) are important protection devices. Study [21–22] investigated coordination optimization for the time dial setting and pickup current of DORs, but it did not include the performance of the directional relays themselves. The authors in [23] studied the failure problem of directional relays applied in the microgrid and proposed a new directional relay based on the amplitude of the measured impedance. This method was applicable to different voltage levels and was not affected by the fault resistance. However, its performance may be affected in the case of weak output of power plants due to lack of power frequency components during a fault. In addition, for high-voltage transmission line, fault component based directional relays are key elements of directional longitudinal protection and their adaptability analysis was reported in [24]. The ratio of sequence voltage and sequence current fault components was used to calculate the equivalent sequence superimposed impedances of a system in the study, and it was found that the positive- and negative-sequence superimposed impedances were no longer equal. However, expressions for the equivalent sequence superimposed impedances were not deduced in this study, and the influence mechanism of fault component based directional relays requires further investigation. In [25], a directional relay based on a positive *R-L* model was proposed to determine the direction for wind farms. However, considering that voltage and current signals

This work was supported by the National Key Research and Development Program of China under Grant 2018YFB0904104, by the National Natural Science Foundation of China under Grants 51725702, and 51777071, and by Young Elite Scientists Sponsorship Program by CAST 2018QNRC001. *(corresponding author: Ke Jia.)*

K. Jia, Z. Yang, Y. Fang, and T. Bi are with State Key Laboratory of Alternative Electrical Power System with Renewable Energy Sources, North China Electric Power University, Beijing 102206, China (e-mail: ke.jia@ncepu.edu.cn; mr.yangzhe@outlook.com; yuk.fong@outlook.com; tsbi@ncepu.edu.cn).

M. Sumner is with the University of Nottingham, UK (e-mail: Mark.Sumner@nottingham.ac.uk).

were severely affected by fault current limiters (FCL) during the first quarter cycle after a fault for IIREGs, the time-domain algorithm based directional relays experienced operational challenges [26]. Therefore, a fast frequency-domain based protection scheme is required for an outgoing transmission line.

The main contributions of this paper are: 1) the expressions for the IIREG sequence superimposed impedances are deduced and both angular characteristics are analyzed considering different influencing factors. 2) based on these results, the performance of the fault component based directional relays installed on an outgoing transmission line are studied in detail. 3) to solve the adaptability problem, a protection scheme based on high-frequency impedance is proposed to determine the fault direction with a stable impedance angle. The above-mentioned problems and the proposed scheme are then verified by RTDS simulation and using field testing data.

II. Characteristics Analysis of Equivalent Sequence Superimposed Impedance of IIREGs

The typical topology of an IIREG is provided in Fig. 1, and is composed of a power source, an inverter, an LCL filter, and a step-up transformer. The $\dot{U}$ and $\dot{I}$ are power frequency voltage and current phasors of the IIREG output, respectively.

Fault component based directional relays determine the fault direction according to the phase relationship between power frequency fault components $\Delta\dot{U}$ and $\Delta\dot{I}$. Therefore, the angular characteristics of the ratio of $\Delta\dot{U}$ and $\Delta\dot{I}$ must be analyzed. The ratios of positive- and negative-sequence components of $\Delta\dot{U}$ and $\Delta\dot{I}$ are defined as the equivalent positive- and negative-sequence superimposed impedance ΔZ_1, and ΔZ_2, respectively, as shown in (1) and (2).

$$\Delta Z_1 = \frac{\dot{U}_1 - \dot{U}_b}{-\left(\dot{I}_1 - \dot{I}_b\right)} \tag{1}$$

$$\Delta Z_2 = \frac{\dot{U}_2}{-\dot{I}_2} \tag{2}$$

where the positive direction of the current is outflowing from IIREGs. Subscripts 1, 2, and b represent the positive- and negative-sequence components during a fault and the pre-fault electrical quantities respectively.

Unlike conventional synchronous generators, the IIREG positive- and negative-sequence superimposed impedances are not equal to its equivalent positive- and negative-sequence impedances before and during a fault due to the IIREG variable internal potential and internal impedance. To derive the equivalent positive- and negative-sequence superimposed impedance expressions, it is necessary to know the positive- and negative-sequence voltages and currents of IIREGs before and during a fault.

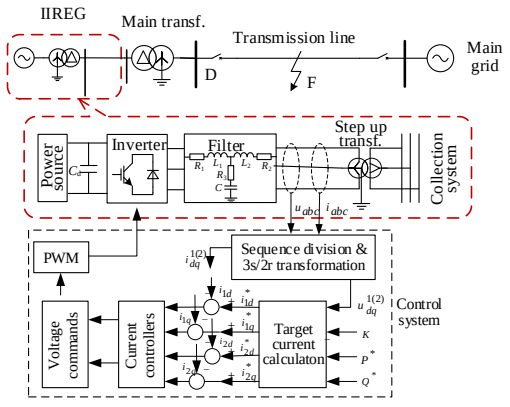

Fig. 1. Simplified diagram of a system connected with the inverter-interfaced renewable energy power plant.

A. Positive- and negative-sequence voltages and currents

As shown in Fig. 1, when an asymmetric fault (this analysis can also apply to symmetrical faults) occurs in an external system, negative-sequence components cause frequency-doubled oscillations in the IIREG output power:

$$\begin{cases} P = P_a + P_{c2}\cos(2\omega t) + P_{s2}\sin(2\omega t) \\ Q = Q_a + Q_{c2}\cos(2\omega t) + Q_{s2}\sin(2\omega t) \end{cases} \tag{3}$$

where P_a and Q_a are average values of the active and reactive powers, P_{c2}, P_{s2}, Q_{c2}, and Q_{s2} are the powers of the frequency-doubled cosine and sine components, and ω is the power frequency electrical angular velocity.

To suppress the oscillations of the fault current injected by IIREGs, the positive- and negative-sequence currents of IIREGs are controlled individually by a positive and negative dq synchronous rotation frame [27]. The above power values are expressed with voltages and currents in the double dq synchronous rotation frame:

$$\begin{bmatrix} P_a \\ P_{c2} \\ P_{s2} \\ Q_a \\ Q_{c2} \\ Q_{s2} \end{bmatrix} = \begin{bmatrix} u_{1d} & u_{1q} & u_{2d} & u_{2q} \\ u_{2d} & u_{2q} & u_{1d} & u_{1q} \\ u_{2q} & -u_{2d} & -u_{1q} & u_{1d} \\ u_{1q} & -u_{1d} & u_{2q} & -u_{2d} \\ u_{2q} & -u_{2d} & u_{1q} & -u_{1d} \\ -u_{2d} & -u_{2q} & u_{1d} & u_{1q} \end{bmatrix} \begin{bmatrix} i_{1d} \\ i_{1q} \\ i_{2d} \\ i_{2q} \end{bmatrix} \tag{4}$$

where all quantities are per unit values. The base values of the voltage u and the current i are the peak values of the rated phase voltage u_{Nm} and current i_{Nm} of the IIREG respectively. The subscripts d and q represent the electrical quantities in the dq frame.

As the four current variables cannot control six power amplitudes simultaneously in (4), only four of them (or two negative-sequence currents) can be controlled. Three control strategies exist: 1) eliminating the negative-sequence current (i_{2d}=i_{2q}=0), 2) eliminating reactive power oscillations (Q_{c2}=Q_{s2}=0) and 3) eliminating active power oscillations (P_{c2}=P_{s2}=0). Under different control strategies, reference currents can be calculated as (5) [28]:

$$\begin{bmatrix} i_{1d}^* \\ i_{1q}^* \\ i_{2d}^* \\ i_{2q}^* \end{bmatrix} = \begin{bmatrix} u_{1d} & u_{1q} \\ u_{1q} & -u_{1d} \\ -Ku_{2d} & Ku_{2q} \\ -Ku_{2q} & -Ku_{2d} \end{bmatrix} \begin{bmatrix} \frac{P_a^*}{M} \\ \frac{Q_a^*}{N} \end{bmatrix} \tag{5}$$

where superscript * indicates the reference values, and P_a^*, Q_a^* are reference values for the active and reactive powers. The three different values (0, 1, -1) of coefficient K corresponds to the previously-mentioned three FRT control strategies, respectively. The variables M, N satisfy the equations: $M=(u_{1d})^2+(u_{1q})^2-K(u_{2d})^2-K(u_{2q})^2$ and $N=(u_{1d})^2+(u_{1q})^2+K(u_{2d})^2+K(u_{2q})^2$.

The positive- and negative-sequence short-circuit currents of IIREGs can be obtained by the current reference values in (5) through coordinate transformation:

$$\begin{cases} i_{1\phi} = i_{1\mathrm{m}} \cos(\omega t - \omega t_0 + \varphi_{1\mathrm{i}} + \varphi_{\phi}) \\ i_{2\phi} = i_{2\mathrm{m}} \cos(\omega t - \omega t_0 - \varphi_{2\mathrm{i}} - \varphi_{\phi}) \end{cases}, t \geq t_0 \tag{6}$$

where $i_{1\phi}$, $i_{2\phi}$, $i_{1\mathrm{m}}$, and $i_{2\mathrm{m}}$ are actual values, and $i_{1\mathrm{m}}=|i_{1\mathrm{d}}^*+\mathrm{j}i_{1\mathrm{q}}^*|\times i_{\mathrm{Nm}}$, $i_{2\mathrm{m}}=|i_{2\mathrm{d}}^*+\mathrm{j}i_{2\mathrm{q}}^*|\times i_{\mathrm{Nm}}$. $|\cdot|$ indicates the modulus of a complex number. Subscript ϕ is the fault phase, m denotes the peak value, and t_0 is the fault time. Here, $\varphi_{1\mathrm{i}}=\arctan(i_{1\mathrm{q}}^*/i_{1\mathrm{d}}^*)$, $\varphi_{2\mathrm{i}}=\arctan(i_{2\mathrm{q}}^*/i_{2\mathrm{d}}^*)$, and the range of all angles is specified between -180° and 180°. φ_{a}=0°, φ_{b}=-120°, and φ_{c}=120°.

Similarly, the positive- and negative-sequence voltages of the IIREG output are:

$$\begin{cases} u_{1\phi} = u_{1\mathrm{m}} \cos(\omega t - \omega t_0 + \varphi_{1\mathrm{u}} + \varphi_{\phi}) \\ u_{2\phi} = u_{2\mathrm{m}} \cos(\omega t - \omega t_0 - \varphi_{2\mathrm{u}} - \varphi_{\phi}) \end{cases}, t \geq t_0 \tag{7}$$

where $u_{1\phi}$, $u_{2\phi}$, $u_{1\mathrm{m}}$, and $u_{2\mathrm{m}}$ are actual values, $u_{1\mathrm{m}}=|u_{1\mathrm{d}}+\mathrm{j}u_{1\mathrm{q}}|\times u_{\mathrm{Nm}}=k_1 u_{\mathrm{Nm}}$, and $u_{2\mathrm{m}}=|u_{2\mathrm{d}}+\mathrm{j}u_{2\mathrm{q}}|\times u_{\mathrm{Nm}}=k_2 u_{\mathrm{Nm}}$. Here, k_1 and k_2 are drop coefficients of positive- and negative-sequence voltages, both of which range from 0 to 1. Additionally, $\varphi_{1\mathrm{u}}=\arctan(u_{1\mathrm{q}}/u_{1\mathrm{d}})$, and $\varphi_{2\mathrm{u}}=\arctan(u_{2\mathrm{q}}/u_{2\mathrm{d}})$.

B. Positive-sequence superimposed impedance

It is known from (6) and (7) that positive-sequence voltage and current phasors can be expressed as:

$$\begin{cases} \dot{U}_{1\phi} = \dfrac{k_1 u_{\mathrm{Nm}}}{\sqrt{2}} \mathrm{e}^{\mathrm{j}(\varphi_{1\mathrm{u}} + \varphi_{\phi})} \\ \dot{I}_{1\phi} = \dfrac{i_{1\mathrm{m}}}{\sqrt{2}} \mathrm{e}^{\mathrm{j}(\varphi_{1\mathrm{i}} + \varphi_{\phi})} \end{cases} \tag{8}$$

To avoid the oscillations of the grid voltage, IIREGs generally operate at unity power factor. In the meantime, considering the equivalent impedance angle difference of the grid-connected system between normal operation and a fault, the pre-fault voltage and current phasors can be expressed as:

$$\begin{cases} \dot{U}_{\mathrm{b}\phi} = \dfrac{u_{\mathrm{Nm}}}{\sqrt{2}} \mathrm{e}^{\mathrm{j}(\varphi_{1\mathrm{u}} + \varphi_{\phi} - \Delta\theta)} \\ \dot{I}_{\mathrm{b}\phi} = \dfrac{k_3 i_{\mathrm{Nm}}}{\sqrt{2}} \mathrm{e}^{\mathrm{j}(\varphi_{1\mathrm{u}} + \varphi_{\phi} - \Delta\theta)} \end{cases} \tag{9}$$

where $\Delta\theta$ is the angular difference of positive-sequence voltages before and during the fault. k_3 (load factor) is defined as the ratio of a load current and the rated current, and the value ranges from 0 to 1. The load current is the current injected by IIREGs before the fault.

Substituting (8) and (9) into (1), the amplitude and the phase angle of the IIREG equivalent positive-sequence superimposed impedance is calculated as follows:

$$\left|\Delta Z_{1\phi}\right| = \frac{\dfrac{u_{\mathrm{Nm}}}{i_{\mathrm{Nm}}} \sqrt{1 + \dfrac{1}{(k_1)^2} - \dfrac{2\cos\Delta\theta}{k_1}}}{\sqrt{\dfrac{P_{\mathrm{a}}^{*2}}{M^2} + \dfrac{Q_{\mathrm{a}}^{*2}}{N^2} + \dfrac{k_3}{k_1}\left(\dfrac{k_3}{k_1} - \dfrac{2P_{\mathrm{a}}^*}{M}\cos\Delta\theta - \dfrac{2Q_{\mathrm{a}}^*}{N}\sin\Delta\theta\right)}} \tag{10}$$

$$\arg\Delta Z_{1\phi} = \arctan \frac{\dfrac{Q_{\mathrm{a}}^*}{N}\cos\Delta\theta - \left(\dfrac{P_{\mathrm{a}}^*}{M} - k_3\right)\sin\Delta\theta - k_1\dfrac{Q_{\mathrm{a}}^*}{N}}{\dfrac{Q_{\mathrm{a}}^*}{N}\sin\Delta\theta + \dfrac{P_{\mathrm{a}}^*}{M}\cos\Delta\theta - \dfrac{k_3}{k_1}} \Bigg/ \frac{k_3\cos\Delta\theta - k_1\dfrac{P_{\mathrm{a}}^*}{M}}{\dfrac{Q_{\mathrm{a}}^*}{N}\sin\Delta\theta + \dfrac{P_{\mathrm{a}}^*}{M}\cos\Delta\theta - \dfrac{k_3}{k_1}} + 1 \tag{11}$$

where arg ( ) represents the phase angle of a phasor.

The two-argument (the imaginary and the real component of the impedance) inverse tangent function is used, so (11) cannot be further simplified. The amplitude and the phase angle of the IIREG equivalent positive-sequence superimposed impedance are both related to K, P_{a}^*, Q_{a}^*, $u_{1\mathrm{d}}$, $u_{1\mathrm{q}}$, $u_{2\mathrm{d}}$, $u_{2\mathrm{q}}$, $\Delta\theta$, and k_3. Therefore, they are closely related to the FRT control strategies, fault conditions and load currents.

The performance of fault component based directional relays is determined by the impedance angle, thus the impedance angle in (11) is analyzed for different influencing factors.

If $\Delta\theta$ is less than 5°, it can be approximated as $\cos\Delta\theta$=1, $\sin\Delta\theta$=0. Compared with cos5° and sin5°, the errors are and 0.38% and 8.7%, respectively, and both are less than 10%. The errors are small and this approximation can be accepted in the field of protection. In this circumstance, (11) can be simplified as:

$$\arg\Delta Z_{1\phi} = \arctan\frac{Q_{\mathrm{a}}^*/N}{P_{\mathrm{a}}^*/M - k_3/k_1} \tag{12}$$

When K=0, M and N both equal $(k_1)^2$, which are always larger than 0. Considering that IIREGs output reactive powers during a fault, Q_{a}^* will be also larger than 0, then $Q_{\mathrm{a}}^*/N>0$, so the range of $\arg\Delta Z_{1\phi}$ is between 0° and 180° in any fault scenario. Furthermore, if $P_{\mathrm{a}}^*/M-k_3/k_1>0$, regardless of the decrease of Q_{a}^* and k_3 (or the increase of P_{a}^* and k_1), $\arg\Delta Z_{1\phi}$ will decrease continuously until close to 0°. If $P_{\mathrm{a}}^*/M-k_3/k_1<0$, regardless of the decrease of Q_{a}^*, P_{a}^*, and k_1 (or the increase of k_3), $\arg\Delta Z_{1\phi}$ will increase continuously until close to 180°.

When K=1, N equals $(k_1)^2+(k_2)^2$ and is larger than 0. Likewise, Q_{a}^*/N will also be larger than 0. In this circumstance, $\arg\Delta Z_{1\phi}$ ranges from 0° to 180° in any fault scenario. In particular, $\arg\Delta Z_{1\phi}$ will approach 0° (or 180°) if Q_{a}^*/N is much smaller than the absolute value of $P_{\mathrm{a}}^*/M-k_3/k_1$.

When K=-1, the sign of $N=(k_1)^2-(k_2)^2$ is uncertain. In the case of $Q_{\mathrm{a}}^*/N>0$, $\arg\Delta Z_{1\phi}$ ranges from 0° to 180°. Furthermore, $\arg\Delta Z_{1\phi}$ will approach 0° (or 180°) if Q_{a}^*/N is much smaller than the absolute value of $P_{\mathrm{a}}^*/M-k_3/k_1$. For $Q_{\mathrm{a}}^*/N<0$, $\arg\Delta Z_{1\phi}$ will be between -180° and 0° and other analysis is similar as the above.

If $\Delta\theta$ is larger than 5°, (11) cannot be further simplified. The phase angle of the positive-sequence superimposed impedance is a variable value under different influencing factors.

In summary, as the phase angle of the IIREG equivalent positive-sequence superimposed impedance is affected by the FRT control strategies, fault conditions, and load currents, it is no longer constant. In such circumstances, the phase angle sometimes approaches 0° (or 180°) and can range from -180° to 0°.

C. Negative-sequence superimposed impedance

The amplitude and the phase angle of the IIREG equivalent negative-sequence superimposed impedance can be calculated by substituting the negative-sequence components of (6) and (7) into (2):

$$\left|\Delta Z_{2\phi}\right| = \frac{u_{\mathrm{Nm}}}{i_{\mathrm{Nm}}\left|K\right|\sqrt{\dfrac{P_{\mathrm{a}}^{*2}}{M^2} + \dfrac{Q_{\mathrm{a}}^{*2}}{N^2}}} \tag{13}$$

$$\arg\Delta Z_{2\phi} = \arctan\frac{-KQ_{\mathrm{a}}^*/N}{-KP_{\mathrm{a}}^*/M} - 180^\circ \tag{14}$$

It can be seen from the above expressions that the

amplitude and the phase angle of the IIREG equivalent negative-sequence superimposed impedance are only related to the control strategies and fault conditions.

When K=0, negative-sequence current injected by IIREGs is zero, so the equivalent negative-sequence superimposed impedance is infinite. When K=1 or K=-1, the analytical method is similar to that used for the analysis of the positive-sequence superimposed impedance. It can be concluded that the phase angle of the IIREG equivalent negative-sequence superimposed impedance is no longer constant, sometimes approaches 0° (or 180°) and can even exist in the range of -180° to -90°.

III. THE FAULT COMPONENT BASED DIRECTIONAL RELAY

Fault component based directional relays include a positive-sequence fault component based directional relay, a negative-sequence directional relay, a zero-sequence directional relay and a phasor fault component based directional relay.

The positive direction criteria for all kinds of fault component based directional relays can be expressed as:

$$-180^\circ < \arg\frac{\Delta\dot{U}}{\Delta\dot{I}} < 0^\circ \tag{15}$$

For a synchronous system, the impedance angle detected by fault component based directional relays is approximately -90° because the reactance is much larger than the resistance. Therefore, -90° is considered to be the most sensitive angle. In general, the sensitivity is considered to be sufficient when the phase angle ranges from -120° to -60°.

Fault component based directional relays are all installed at the outgoing transmission lines (point D in Fig. 1). When a fault occurs in the interior of the IIREG power plant, the equivalent impedance measured at D is reflected by the impedance characteristics of the traditional synchronous system. In this case, fault component based directional relays operate correctly. When a fault occurs at the outgoing transmission line or the main grid, the equivalent impedance measured at D is reflected by the impedance characteristics of IIREGs. It can be seen from the above analysis that the phase angles of the IIREG equivalent positive- and negative-sequence superimposed impedances change from -180° to 180° in different fault scenarios. This will affect the performance of fault component based directional relays.

A. Positive-sequence fault component based directional relay

For a fault on the protected transmission line, seen from the relay point D, the system fault additional network is shown in Fig. 2. Here, n_1 and n_2 are transformer ratios of the step-up transformer and the main transformer, respectively, while Z_{t1}, Z_{l1}, and Z_{T1} are positive-sequence impedances of the step-up transformer, the collection line, and the main transformer, respectively.

The positive-sequence superimposed impedance $\Delta Z_{D1\phi}$ can be calculated by the voltages and currents before and during the fault measured at D and (1). At the same time, the fault additional network shows determining this impedance can be expressed as:

$$\Delta Z_{D1\phi} = -n_1^2 n_2^2 \Delta Z_{1\phi} - n_2^2 Z_{t1} - n_2^2 Z_{l1} - Z_{T1} \tag{16}$$

where subscript D indicates the installation location of the directional relay.

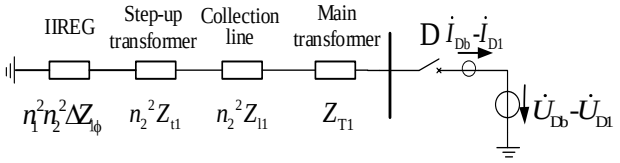

Fig. 2. System fault additional network.

Considering the ratio of the step-up transformer and the main transformer, the IIREG equivalent positive-sequence superimposed impedance is often much larger than the positive-sequence impedance of other elements. The impedance angle calculated by positive-sequence fault component based directional relay approximately satisfies:

$$\arg\Delta Z_{D1\phi} = \arg\Delta Z_{1\phi} - 180^\circ \tag{17}$$

In combining (15) and (17), it can be concluded that if $\arg\Delta Z_{1\phi}$ is between 0° and 180°, it is regarded as a positive direction fault. However, according to the analysis in Section II, $\arg\Delta Z_{1\phi}$ can be close to 0° (or 180°), and sometimes ranges from -180° to 0°. Therefore, a positive-sequence fault component based directional relay will refuse to operate or its sensitivity may be insufficient.

B. Negative-sequence directional relay

When K=0, IIREGs do not output negative-sequence current, so the negative-sequence directional relay cannot operate normally. When K=±1, the derivation process of $\arg\Delta Z_{D2\phi}$ is the same as (17):

$$\arg\Delta Z_{D2\phi} = \arg\Delta Z_{2\phi} - 180^\circ \tag{18}$$

Combining (15), (18) and the analysis in section II, it can be concluded that the sensitivity of the negative-sequence directional relay might decrease greatly or the relay will fail to operate.

C. Zero-sequence directional relay

For asymmetric grounding faults located at F, the impedance calculated by the zero-sequence directional relay is reflected by impedance characteristics of the main transformer, which is not affected by IIREGs. Therefore, it can operate correctly.

D. Phasor fault component based directional relay

Phasor fault component based directional relays can be classified into a single phasor fault component based directional relay and a phasor difference fault component based directional relay. The former is mainly used for a single-phase to ground fault and the latter is mainly used for a phase fault.

To analyze the performance of a single phasor fault component based directional relay, a phase-A to ground fault at F (Fig. 2) is used for demonstration. According to (17), the impedance angle $\arg\Delta Z_{DA}$ calculated by the directional relay can be obtained approximately as:

$$\arg\Delta Z_{DA} = \arg\left(-\frac{\Delta Z_{1A}\Delta\dot{I}_{1A}e^{j\theta} + \Delta Z_{2A}\dot{I}_{2A}e^{j\sigma}}{\Delta\dot{I}_{1A}e^{j\theta} + \dot{I}_{2A}e^{j\sigma}}\right) \tag{19}$$

where subscript A indicates the fault phase is phase-A, and σ is the conversion angle after negative-sequence current flows through the step-up transformer and the main transformer.

When K=0, IIREGs do not output negative-sequence current. In this case, (19) is the same as (17), so the directional relay has the same problem as the positive-sequence fault component based directional relay. When K=±1, (19) is affected by angular characteristics of the IIREG equivalent positive- and negative-sequence superimposed impedances.

In this situation the sensitivity of the directional relay will decrease or the relay will fail to operate. In addition, the phasor difference component based directional relay also encounters a similar problem.

To summarize, sequence and phasor fault component based directional relays (except zero-sequence directional relay) may fail to operate, and a more reliable and accurate solution is proposed below.

IV. An Improved Protection Scheme

According to the above analysis, directional relays face operational challenges due to the variable fault impedance characteristics of IIREGs. This problem can be solved in two ways. One is to optimize the control system to maintain a fixed impedance angle during the fault. However, since the active and reactive powers vary according to the voltage drop depending on FRT requirements, the impedance angle of IIREGs might not be controlled to a stable value and this can still lead to relay malfunction. The other one is to improve the protection algorithm. The phase angle of the IIREG's high-frequency impedance is stable at around 90° and it is not significantly affected by the control system because the selected frequency range is higher than the bandwidth of the current loop. Owing to this, a high-frequency impedance-based protection scheme is proposed to determine the fault direction.

A. *High-frequency impedance of the IIREG*

When a fault occurs at F (Fig. 2), the voltage drop can be seen as a step signal (the direction of the voltage during a fault is opposite to that during the normal operation) injected at the fault location. For the step signal in Fig. 3 (a), its amplitude result after Laplace transform is shown in Fig. 3 (b). Theoretically, it possesses wideband frequency information, and the high frequency components can be extracted by wavelet transform from a short data window of 10ms, which includes 5ms of data during the fault inception.

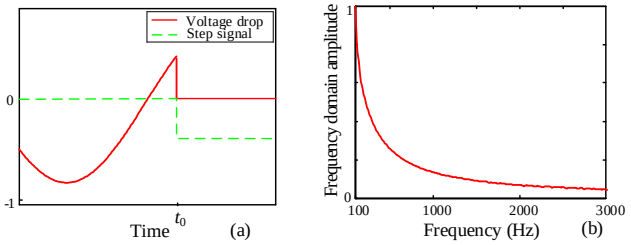

Fig. 3. A step signal and its Laplace transform. (a) A step signal, (b) Amplitude result after Laplace transform.

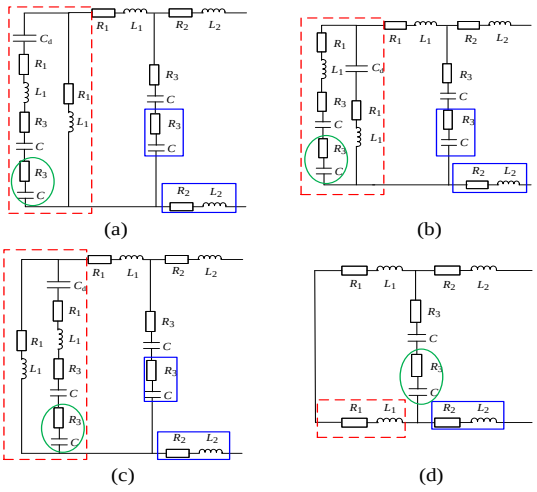

Fig. 4. High frequency impedance structures.

The high-frequency impedance model of the IIREG for phase to phase faults has been studied in [29], providing four impedance structures under different switching conditions, as shown in Fig. 4.

In the four structures, only the parts in the red dashed box are different and are connected in series with R_1 and L_1, then in parallel with the filter capacitor branch, and finally in series with R_2 and L_2. In the high frequency range, the large capacitance C_d can be ignored and the impedance value of the filter capacitor branch is much smaller than that of the parallel branch. Under this condition, the total impedance value for the two branches in parallel will be dominated by the filter capacitance. For parallel inductors and capacitors, if the inductive reactance is greater than ten times the capacitive reactance, the inductor branch can be ignored. After ignoring the small resistances, the above condition is satisfied as long as the inductive reactance of L_1 is greater than ten times the capacitive reactance value of $2C$ for the four impedance structures in Fig. 4. Therefore, the selected frequency should satisfy:

$$f > \sqrt{\frac{10}{8\pi^2 L_1 C}} \tag{20}$$

Under the premise of (20), the impedance value of the filter capacitor branch is at least one-fifth or one-twentieth that of the parallel branch. Thus, the parallel branch can be ignored. In the view of impedance angle, the four circuit topologies can be unified as the *RLC* series circuit shown in Fig. 5. For phase to ground faults, the high frequency impedance structures must remove the parts in the blue solid line box, and transfer the parts in the green oval frame to the parallel branch in Fig. 4. To acquire the unified model shown in Fig. 5, the selected frequency should satisfy:

$$f > \sqrt{\frac{10}{4\pi^2 L_1 C}} \tag{21}$$

Compared with (20) and (21), it can be concluded that only (21) is satisfied and the impedance structures can be unified as in Fig. 5 for the above two high-frequency paths.

As shown in Fig. 5, R is equal to R_2+R_3. The phase angle of the total impedance of the unified structure should be more than 60° to give the proposed method high sensitivity. In this circumstance, the frequency should also satisfy:

$$2\pi f L_2 - \frac{1}{2\pi f C} > R\tan 60^\circ \tag{22}$$

Besides, the selected frequency must also be higher than the bandwidth of the current loop in order to avoid influence the control system considering its response time may be less than 5 ms [30-31]. On these bases, the lower limit of frequency is determined.

At the same time, the high-frequency range of interest is preferably below 3 kHz. The reason that 3 kHz limitation is

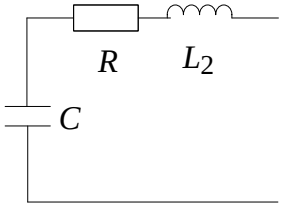

Fig. 5. Unified impedance structure.

used 1) a good signal-to-noise ratio (SNR) is obtained. 2) the limitation of the measurement units and the data processing boards are considered. 3) the system parasitic capacitance can be ignored. 4) the bandwidth of the current loop of inverters installed in the power plant is usually below 3 kHz.

B. The improved scheme

The equivalent circuit for the fault located at the positive direction of the transmission line is shown in Fig. 6. As illustrated in Fig. 6, R_S and L_S represent the equivalent resistance and inductance of the main grid, Z_{line_A} and Z_{line_B} are the high-frequency impedance from the fault location to the two sides of the outgoing transmission line, and the Z_{TC} is the equivalent high-frequency impedance from the point D to the IIREG outlet. Additionally, V_S is the high-frequency voltage source caused by voltage drops, R_g is the fault resistance, and Z_D is calculated high-frequency impedance.

According to the reference direction shown in Fig. 6, the impedance Z_D can be directly calculated using the high-frequency components measured at point D, and can be expressed as:

$$Z_D = \frac{V_D}{I_D} = -Z_{TC} - R - jwL_2 + j\frac{1}{wC} \tag{23}$$

where V_D and I_D are the high-frequency voltage and current measured at point D. For phase faults, V_D=$V_{\phi1}$-$V_{\phi2}$, I_D=$I_{\phi1}$-$I_{\phi2}$ and $\phi1$ and $\phi2$ are the fault phases.

It can be seen from Fig. 6 and (23) that Z_D is only related to the impedance behind point D. Therefore, it is unaffected by R_g and its value mainly depends on the IIREG equivalent model. In the selected high-frequency range, the equivalent model can be approximated to an *RL* series circuit because (22) has ensured that the impedance of inductor L_2 is greater than that of capacitor *C*. According to (23), the phase angle argZ_D calculated by the proposed scheme is a negative value and close to -90°. Therefore, the criteria of the positive direction in (24) is similar to (15).

$$-180^\circ < \arg\frac{V_D}{I_D} < 0^\circ \tag{24}$$

The proposed method can determine all types of faults and operate within several ms. As the selected frequency is higher than the bandwidth of the current loop, this method is essentially unaffected by the control strategies. The method also demonstrates a high sensitivity in the selected frequency range. There must be at least one phase-to-phase high-frequency path or phase to ground high-frequency path for all kinds of faults, so the proposed scheme is effective for all fault types. However, since the method requires a high sampling rate, the protection device on the IIREG side needs to be updated. The flow chart of this scheme is presented in Fig. 7. Here, for fault starting and fault phase selection elements that have already been installed in the power plant can be utilized, such as the phase current fault starting elements and the low voltage phase selector.

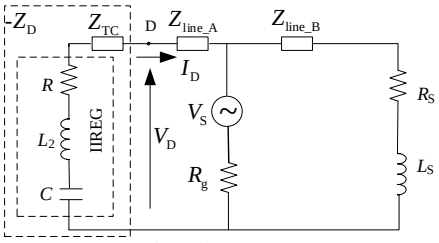

Fig. 6. Equivalent circuit for a fault located at the positive direction.

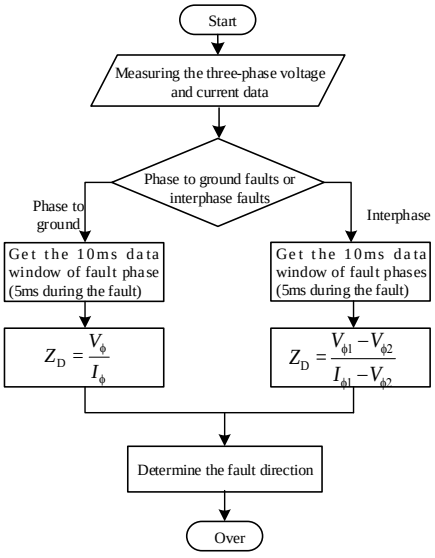

Fig. 7. Flow chart of the proposed method.

V. Simulation Verification and Analysis

To validate the performance of fault component based directional relays and the proposed scheme, experimental tests are carried out on the test platform depicted in Fig. 8. The testing apparatus is composed of four main components: main controller, monitor, PWM generator and RTDS and the function of each part is detailed in [32]. The element parameters are provided in Table A.I, and the fault location of all simulation is set at F in Fig. 1.

A. Theoretical values and simulation values

To verify the derivation of the IIREG positive- and

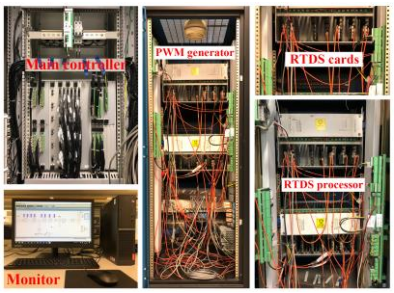

Fig. 8. Physical layout of the experimental test system.

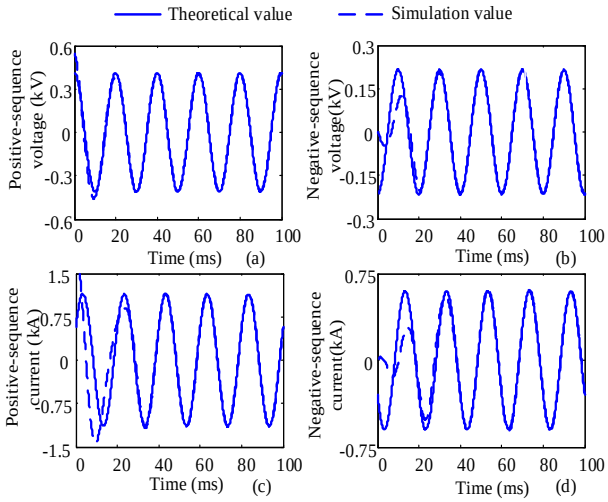

Fig. 9. Simulation and theoretical values of positive- and negative-sequence voltages and currents. (a) Positive-sequence voltage, (b) Negative-sequence voltage, (c) Positive-sequence current, (d) Negative-sequence current.

negative-sequence voltages and currents, simulation parameters are set as follows: K=-1, P_a^*=Q_a^*=0.3 p.u., and k_3=1 p.u.. Fig. 9 shows the simulation results and theoretical values for a phase-A solid grounding fault occurring at F.

As seen in Fig. 9, the simulation results are slightly different from the theoretical results during early stage of the fault. This is because the control system has a dynamic adjustment process after the fault inception considering the controller response time. After this transient period, the simulation results perfectly match the theoretical values.

B. Positive-sequence superimposed impedance

The basic simulation parameters are set as follows: K=0, P_a^*=Q_a^*=0.3 p.u., and k_3=1 p.u.. To verify (12), simulation tests on a phase-A grounding fault are implemented and the results are shown in Fig. 10.

According to Fig. 10(a)~(b), for the solid fault, $\Delta\theta$ is 4.0° and the phase angle of $\Delta Z_{1\phi}$ is 156.5°. Compared with the theoretical value 147.7° obtained by (12), the error is within 10°. When R_g is equal to 5Ω and 10Ω, $\Delta\theta$ is greater than 5°, and the corresponding phase angles of $\Delta Z_{1\phi}$ are 178.2° and -163.9°, respectively. Compared with the theoretical values 148.3° and 151.4° obtained by (12), the differences are both over 30°. This result demonstrates that (12) is only applicable to smaller angular differences.

The impact of different influencing factors on the phase angle obtained from (12) is illustrated in Fig. 10(c)~(f). As depicted in Fig. 10(c)~(f), the arg$\Delta Z_{1\phi}$ are all in the range of 0° to 180°, and with the decrease of P_a^*, Q_a^*, and the increase of k_3, arg$\Delta Z_{1\phi}$ increases and approaches 180°. Additionally, in Fig. 10(c)~(d), the phase angles jump up and down in the case of 0.1 p.u.. This is because the phase angles are all specified between -180° to 180°, and it is considered to be -180° once the phase angle crosses the negative half of the x-axis in the complex plane. These simulation results are consistent with the theoretical analysis.

C. Negative-sequence superimposed impedance

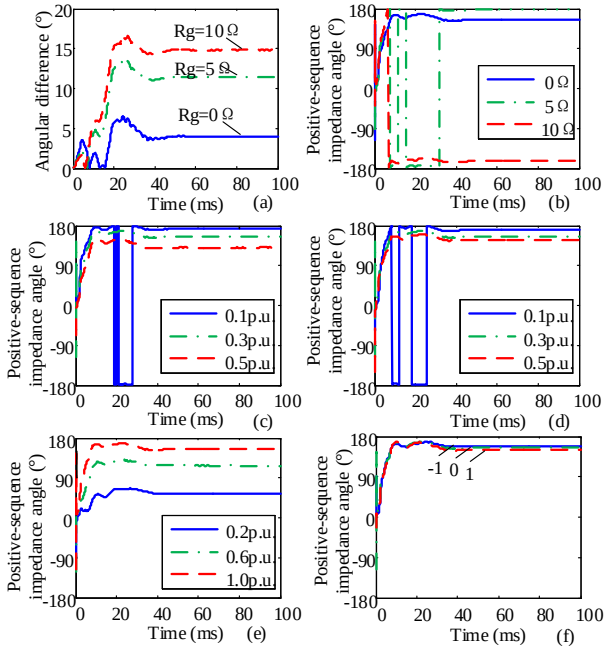

Fig. 10. Angular features of $\Delta Z_{1\phi}$ with different influence factors. (a) Angular differences of positive-sequence voltage, (b) Fault resistances, (c) Active power reference values, (d) Reactive power reference values, (e) Load currents, (f) Control strategies.

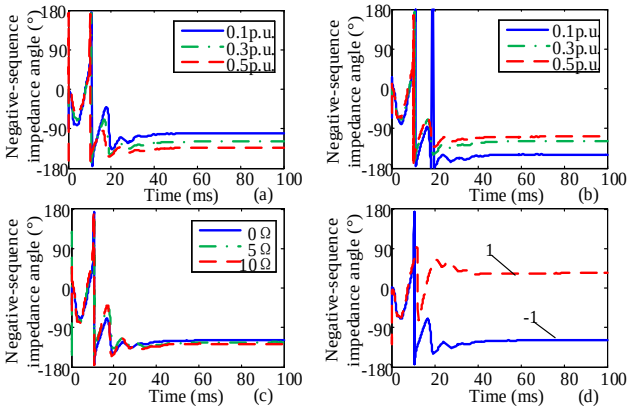

Fig. 11. Angular features of $\Delta Z_{2\phi}$ with different influence factors. (a) Active reference values, (b) Reactive reference values, (c) Fault resistances, (d) Control strategies.

The variation of the phase angles of $\Delta Z_{2\phi}$ is shown in Fig. 11 when a phase-A to ground fault occurs at F. The basic simulation conditions are: P_a^*=Q_a^*=0.3 p.u., R_g=0 Ω, and K=-1.

arg$\Delta Z_{2\phi}$ is between 0° and 180° considering a synchronous system, and the negative-sequence directional relay can operate correctly. However, as seen in Fig. 11(a)~(c), arg$\Delta Z_{2\phi}$ of IIREGs are all in the range of -180° to -90° at steady state. Therefore, the directional relay will refuse to operate. Fig. 11(d) shows that arg$\Delta Z_{2\phi}$ is between 0° and 180° but deviates from 90° when K is set to 1. In this case, the sensitivity of the negative-sequence directional relay will decline. The above conclusions are consistent with the theoretical analysis.

D. Fault component based directional relays

The performance of fault component based directional relays under different influencing factors for the phase-A to ground fault is illustrated in Fig. 12. The PD denotes the positive direction and the ID denotes the inverse direction.

It can be seen from Fig. 12(a)~(b) that zero-sequence

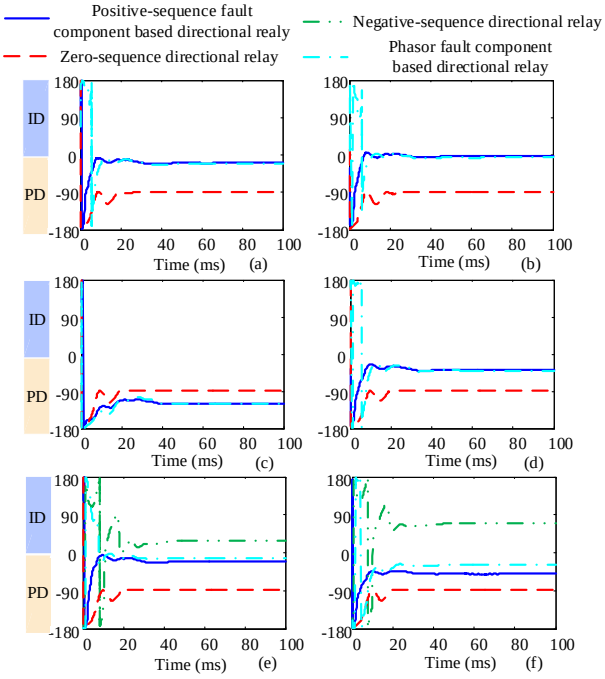

Fig. 12. Performance of different types of fault component based directional relays under different influence factors. (a) K=0, R_g=5 Ω, (b) K=0, R_g=10 Ω, (c) K=0, k_3=0.2 p.u., (d) K=0, k_3=1.0 p.u., (e) K=-1, Q_a*=0.1 p.u., (f) K=-1, Q_a*=0.5 p.u.

directional relay can operate correctly. However, the impedance angles calculated by other directional relays are close to 0°, and their sensitivity must decrease greatly or the relay may refuse to operate.

The simulation results for the effect of load currents are shown in Fig. 12(c)~(d). The impedance angles calculated by positive-sequence and phasor fault component based directional relays are the same and deviate from -90°. This occurrence will cause a decline in sensitivity but the relays can still operate correctly. This is because the current will increase greatly under light load during the fault (maximum to the current limiting value), but the voltage drop essentially has nothing to do with load current. Therefore, it can be known from (1) that the impedance characteristics of IIREGs will be weakened. As seen in Fig. 12(e)~(f), the impedance angles calculated by positive-sequence and phasor fault component based directional relays are no longer the same due to the presence of a negative-sequence current but both approach 0° as the reactive reference value decreases. Therefore, the relays may refuse to operate, and the negative-sequence directional relay also experiences the same problem.

E. The improved scheme

To verify the improved protection scheme, basic simulation parameters are set as follows: $P_a^*=Q_a^*=0.3$ p.u., and $k_3=1$ p.u.. In addition, the sampling frequency is set to 20 kHz to fully reflect the high-frequency information of a fault. As the high-frequency loops have only phase-to-phase and phase-to-ground paths, the effectiveness of the proposed method is verified by phase-B-to-phase-C faults (BC) and phase-A grounding fault (AG).

Fig. 13 illustrates the high-frequency impedance angles calculated by the proposed relay under different control strategies. The switching frequency of the converter is 5 kHz, so the selected frequency should be greater than 0.5 kHz considering the bandwidth of the current loop is usually one tenth of the switching frequency. In addition, for the phase-to-phase paths and phase to ground paths, the lower frequency limits calculated according to (20) and (21) are 759 Hz and 1073 Hz respectively. It can be seen from Fig. 13(a)~(b) that the phase angles tend to be stable in their respective selected frequency range. Additionally, all the impedance angles in Fig. (13) are close to -90° in the common frequency range above 1 kHz. These findings illustrate that the proposed scheme is not affected by different control strategies.

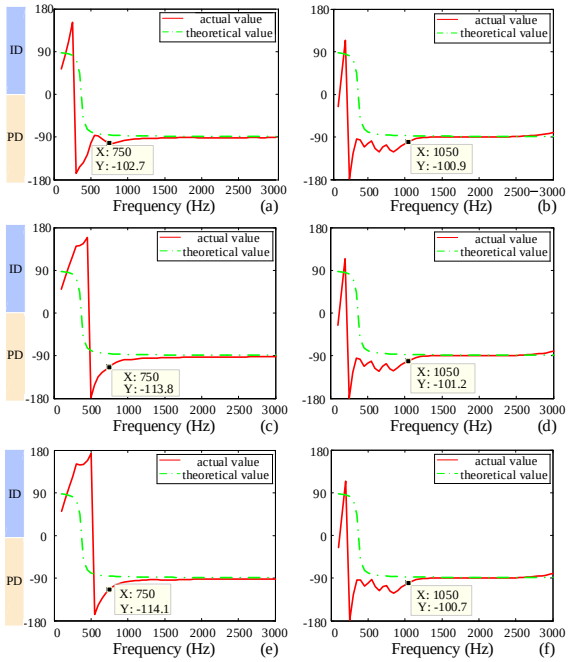

Fig. 13. Performance of the proposed method under two-phase faults and phase to ground faults. (a) K=0, BC, (b) K=0, AG, (c) K=1, BC, (d) K=1, AG, (e) K=-1, BC, (f) K=-1, AG.

Furthermore, to verify the effect of the fault resistance, R_g is set to 0 Ω, 5Ω, and 10Ω respectively and K is set to 0. As observed from Fig. 14, all three curves essentially coincide in the high-frequency range of interest and are stable at -90°. Therefore, the fault resistance has little impact on the proposed scheme.

Additionally, as the selected frequency range in Fig. 14 is below 3 kHz, the sampling frequency must be above 6 kHz according to the sampling theorem. To verify the effect of the sampling frequency, the sampling frequency is set to 10 kHz, 20 kHz, and 50 kHz respectively for K=0.

As seen from Fig. 15, the phase angles at three different sampling frequencies are essentially the same. However, for a 3 kHz waveform, there are only 3 points per cycle at a sampling frequency of 10 kHz. Therefore, considering the calculation accuracy and the sampling frequency of the data processing boards, it is appropriate to set the sampling frequency to 20 kHz.

In conclusion, the positive-sequence and phasor fault component based directional relays and negative-sequence directional relay are likely to fail to operate due to a variable impedance angle while the proposed scheme can operate correctly.

VI. Field Testing Data Analysis

The field testing data is derived from a 99 MW wind farm in Jilin, an 850 MW PV power plant (its capacity is largest in the world) in Qinghai and a PV power plant in Jiangxi, respectively. The wind farm is composed of 66 permanent magnet synchronous generators (PMSGs), with a topology the same as that depicted in Fig. 1, and its parameters are provided in Table A.II. A phase-C grounding fault occurs at the main grid and the directional relays are installed at D. For the PV power plant in Qinghai, electricity is collected through 35 kV collection lines and is transported by 330kV sending lines. Detailed topology and parameters for the Qinghai plant are depicted in Fig 16 and table A.III. A phase-B-to-phase-C

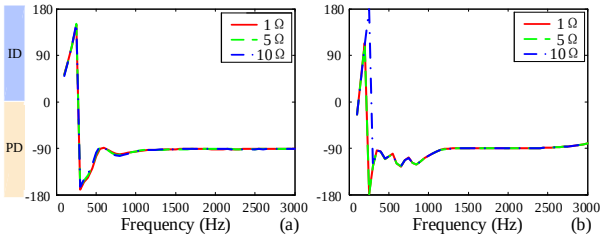

Fig. 14. Performance of the proposed method under different fault.

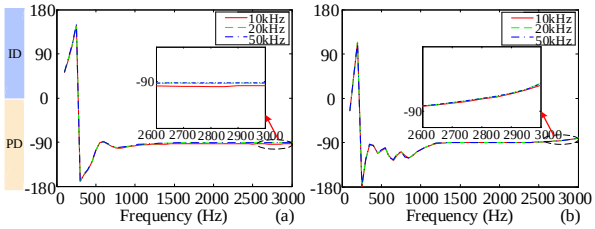

Fig. 15. Performance of the proposed method under different sampling frequencies. (a) BC, (b) AG.

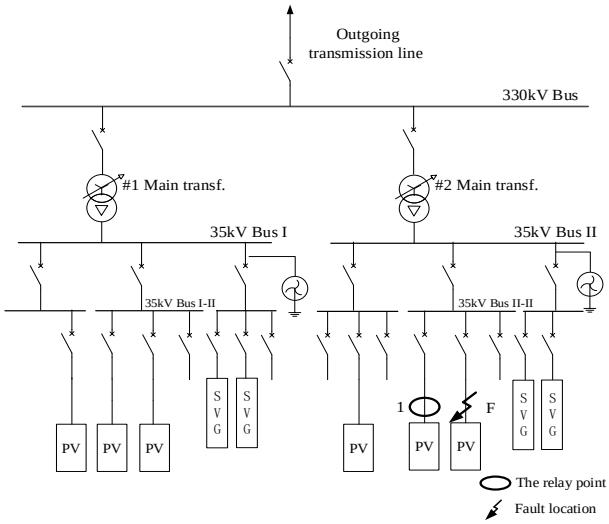

Fig. 16. Detailed topology of the PV power plant in Qinghai.

fault occurs at the collection line, and the relay point is located at the IIREG outlet (location 1 in Fig 16). In addition, the PV power plant in Jiangxi is connected to a 35kV distribution network by a 3.924 km special line. A phase-B-to-phase-C fault occurs at the PV side of the special line.

Data from the wind farm in Jilin is used to confirm the existing problem and effectiveness of the proposed method for phase to ground faults. Fig. 17(a)~(b) provides the sequence currents of the IIREG side and the performance of directional relays respectively. As seen in Fig. 17(a), the negative-sequence current of the IIREG side during the fault is almost zero, so the negative-sequence directional relay cannot operate normally. The curves in Fig. 17(b) possess similar trends to those shown in Fig. 8. The impedance angle (about 170°) calculated by positive-sequence fault component based directional relay is very close to that calculated by the phasor fault component based directional relay. In this circumstance, both directional relays will fail to operate. Instead, the conventional zero-sequence directional relay calculates an angle close to -90° which can operate correctly. The effectiveness of the proposed method for phase to ground faults is illustrated in Fig. 18, where the phase angle is close to -90° in the selected high-frequency range. The deviation above 1.6 kHz is due to the sampling rate of only 5

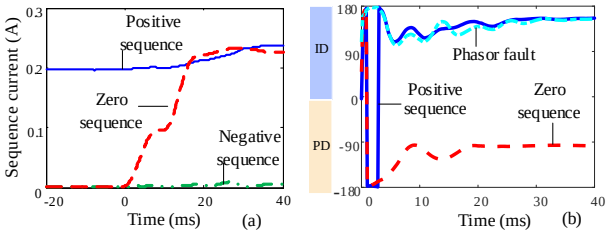

Fig. 17. Performance of different types of fault component based directional relays under field data. (a) Sequence current amplitudes, (b) Action performance.

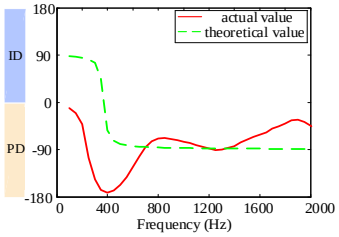

Fig. 18. Performance of the proposed method for phase to ground faults.

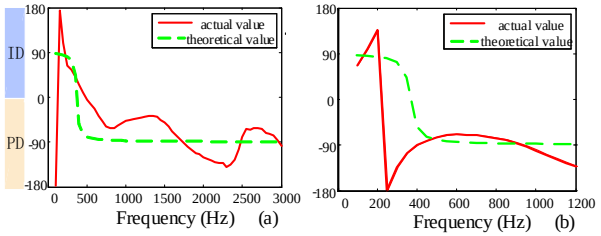

Fig. 19. Performance of the proposed method for phase faults. (a) Qinghai, (b) Jiangxi.

kHz.

The other two sets of field data are used to verify the effectiveness of the proposed method for phase-to-phase faults. The phase angles of high-frequency impedance are provided in Fig. 19.

As seen from Fig.19, the phase angles are located at -180° and 0° in the high-frequency range, confirming the proposed method. However, the angles fluctuate at -90° because the sampling frequencies of the field testing data are only 20/3 kHz and 3.2 kHz, respectively, and this affects the extraction of high-frequency components. The results would match more accurately if the wave-recording device of the PV power plants had a higher sampling frequency.

VII. Conclusions

This study determined expressions for IIREG sequence superimposed impedances and analyzed the impact of different influencing factors. Theoretical analysis and simulation results show that sequence superimposed impedance angles are no longer constant at 90°, and may cause fault component based directional relays (except zero-sequence directional relay) sensitivity decline or failure in operation. To manage this issue, a high-frequency impedance based directional relay was proposed to determine the direction for all types of faults.

The proposed method avoids the influence of fault resistance and low frequency distortions, and the selected frequency is higher than the bandwidth of the current loop, so it is not significantly affected by the control system. These aspects ensure that the proposed method has a stable phase angle of approximately -90°, and meets the requirement of reliability, selectivity, speed and sensitivity. The existing problems and the proposed solution are verified by the RTDS simulation and using field testing data.

Appendix

Table A.I
Simulation Parameters

Element	Parameter	Value
Outgoing transmission line	Voltage level	220 kV
	Length	40 km
	Positive-sequence impedance	0.076+j0.338 Ω/km
	Zero-sequence impedance	0.284+j0.824 Ω/km
	Positive-sequence capacitance	0.0086 F/km
	Zero-sequence capacitance	0.0061 F/km
Main grid	Equivalent sequence impedances	0.1+j3.1416 Ω
LCL filter	Capacitor	200 μF
	Inductance	1100/924 μH
	Resistance	0.0001/0.0001/0.25Ω
Main transf.	Rated capacity	100 MVA
	Rated transformation ratio	220/35 kV
	Wire connection	YNd
	Short circuit impedance	6%
Step-up transf.	Rated capacity	1.6 MW
	Wire connection	Dyn

	Short circuit impedance	6.76%
Collection line	Equivalent impedance	0.11+j0.129 Ω
IIREG power plant	Unit capacity	1.5 MW
	Installed number	66
PI controller	Coefficients of the voltage loop	0.35 p.u.
	Coefficients of the current loop	0.1 p.u.
	Integral time constant	0.01 p.u.
DC bus	Rated voltage	1.2 kV
	Capacitance	4500 μF

TABLE A.II
DEVICE PARAMETERS OF THE WIND FARM

Unit capacity	1.5 MW
Installed number	66
Rated capacity of main transformer	100 MVA
The number of main transformer	1
Voltage level of outgoing transmission line	220 kV
The length of outgoing transmission line	25.461 km

TABLE A.III
DEVICE PARAMETERS OF THE PV POWER PLANT

Element	Parameter	Value
Outgoing transmission line	Voltage level	330 kV
	Length	42 km
Main transf.	Rated capacity	100 MVA
	Rated transformation ratio	240/35 kV
	Wire connection	YNd11
	Short circuit impedance	13.63%
Step-up transf.	Rated capacity	1000/500-500 kVA
	Rated transformation ratio	37±2×2.5%/0.3-0.3 kV
	Wire connection	Yd11-d11
	Short circuit impedance	6.23%

REFERENCES

[1] B. Shyam and P. Kanakasabapathy, "Renewable energy utilization in India — policies, opportunities and challenges," *2017 International Conference on TAP Energy*, Kollam, 2017, pp. 1-6.

[2] G. Ren, J. Liu, J. Wan, et al., "Overview of wind power intermittency: Impacts, measurements, and mitigation solutions, " in *Applied Energy*, vol. 204, pp. 47-65, Oct. 2017.

[3] P. S. Georgilakis, "Technical challenges associated with the integration of wind power into power systems," *Renewable and Sustainable Energy Reviews*, vol 12, no. 3, pp. 852-863, 2008.

[4] J. Koppinen, J. Kukkola and M. Hinkkanen, "Plug-In Identification Method for an LCL Filter of a Grid Converter," in *IEEE Trans. Ind. Electron.*, vol. 65, no. 8, pp. 6270-6280, Aug. 2018.

[5] X. Fu, S. Li and I. Jaithwa, "Implement Optimal Vector Control for LCL-Filter-Based Grid-Connected Converters by Using Recurrent Neural Networks," in *IEEE Trans. Ind. Electron.*, vol. 62, no. 7, pp. 4443-4454, July 2015.

[6] D. Shin, K. Lee, J. Lee, D. Yoo and H. Kim, "Implementation of Fault Ride-Through Techniques of Grid-Connected Inverter for Distributed Energy Resources With Adaptive Low-Pass Notch PLL," in *IEEE Trans. Power Electron.*, vol. 30, no. 5, pp. 2859-2871, May 2015.

[7] P. Piya, M. Ebrahimi, M. Karimi-Ghartemani and S. A. Khajehoddin, "Fault Ride-Through Capability of Voltage-Controlled Inverters," in *IEEE Trans. Ind. Electron.*, vol. 65, no. 10, pp. 7933-7943, Oct. 2018.

[8] K. Jia, C. Gu, Z. Xuan, l. li and Y. Lin, "Fault Characteristics Analysis and Line Protection Design within a Large-scale Photovoltaic Power Plant," in *IEEE Trans. on Smart Grid*.

[9] A. Camacho, M. Castilla, J. Miret, L. G. de Vicuña and R. Guzman, "Positive and Negative Sequence Control Strategies to Maximize the Voltage Support in Resistive–Inductive Grids During Grid Faults," in *IEEE Trans. Power Electron.*, vol. 33, no. 6, pp. 5362-5373, June 2018.

[10] N. Nimpitiwan, G. T. Heydt, R. Ayyanar and S. Suryanarayanan, "Fault Current Contribution From Synchronous Machine and Inverter Based Distributed Generators," in *IEEE Trans. Power Del.*, vol. 22, no. 1, pp. 634-641, Jan. 2007.

[11] H. Hooshyar and M. Baran, "Fault Analysis on Distribution Feeders With High Penetration of PV Systems,"*2013 IEEE Power & Energy Society General Meeting*, Vancouver, BC, 2013, pp. 1-1.

[12] J. Morren and S. W. H. de Haan, "Short-Circuit Current of Wind Turbines With Doubly Fed Induction Generator," in *IEEE Trans. Energy Convers.*, vol. 22, no. 1, pp. 174-180, March 2007.

[13] S. Pillai and N. Rajasekar, "A Comprehensive Review on Protection Challenges and Fault Diagnosis in PV Systems," in *Renewable and Sustainable Energy Reviews*, vol. 91, pp. 18-40, 2018.

[14] V. Telukunta, J. Pradhan, A. Agrawal, M. Singh and S. G. Srivani, "Protection challenges under bulk penetration of renewable energy resources in power systems: A review," in *CSEE Journal of Power and Energy Systems*, vol. 3, no. 4, pp. 365-379, Dec. 2017.

[15] A. Hooshyar, M. A. Azzouz and E. F. El-Saadany, "Distance Protection of Lines Connected to Induction Generator-Based Wind Farms During Balanced Faults," in *IEEE Trans. Sustainable Energy*, vol. 5, no. 4, pp. 1193-1203, Oct. 2014.

[16] Y. Chen, M. Wen, et al., "Distance Protection for Transmission Lines of DFIG-based Wind Power Integration System," in *International Journal of Electrical Power & Energy Systems*, vol. 100, pp. 438-448, Feb. 2018.

[17] A. Hooshyar, M. A. Azzouz and E. F. El-Saadany, "Distance Protection of Lines Emanating From Full-Scale Converter-Interfaced Renewable Energy Power Plants—Part I: Problem Statement," in *IEEE Trans. Power Del.*, vol. 30, no. 4, pp. 1770-1780, Aug. 2015.

[18] A. Hooshyar, M. A. Azzouz and E. F. El-Saadany, "Distance Protection of Lines Emanating From Full-Scale Converter-Interfaced Renewable Energy Power Plants—Part II: Solution Description and Evaluation," in *IEEE Trans. Power Del.*, vol. 30, no. 4, pp. 1781-1791, Aug. 2015.

[19] B. Han, H. Li, G. Wang, D. Zeng and Y. Liang, "A Virtual Multi-Terminal Current Differential Protection Scheme for Distribution Networks With Inverter-Interfaced Distributed Generators," in *IEEE Trans. on Smart Grid*.

[20] K. Jia, Y. Li, et al., "Transient Current Similarity Based Protection for Wind Farm Transmission Lines, " in *Applied Energy*, vol. 225, pp. 42-51, Sep. 2018.

[21] D. Saha, A. Datta and P. Das, "Optimal coordination of directional overcurrent relays in power systems using Symbiotic Organism Search Optimization technique," in *IET Generation, Transmission & Distribution*, vol. 10, no. 11, pp. 2681-2688, 8 4 2016.

[22] H. H. Zeineldin, H. M. Sharaf, D. K. Ibrahim and E. E. D. A. El-Zahab, "Optimal Protection Coordination for Meshed Distribution Systems With DG Using Dual Setting Directional Over-Current Relays," in *IEEE Trans. on Smart Grid*, vol. 6, no. 1, pp. 115-123, Jan. 2015.

[23] A. Hooshyar and R. Iravani, "A New Directional Element for Microgrid Protection," in *IEEE Trans. on Smart Grid*, vol. 9, no. 6, pp. 6862-6876, Nov. 2018.

[24] J. Tang, G. Song and C. Wang, "Adaptability analysis of directional relays in power systems with wind farms,"*13th International Conference on Development in Power System Protection 2016 (DPSP)*, Edinburgh, 2016, pp. 1-6.

[25] Chenqing Wang, Guobing Song and Jinhua Zhang, "A novel principle of directional relay for wind power integration based on model recognition in time-domain," *2016 IEEE PES Asia-Pacific Power and Energy Engineering Conference (APPEEC)*, Xi'an, 2016, pp. 1851-1855.

[26] H. Jafarabadi Ashtiani, H. Samet and T. Ghanbari, "Evaluation of directional relay algorithms in the presence of FCL," in *IET Science, Measurement & Technology*, vol. 11, no. 6, pp. 713-722, 9 2017.

[27] R. Kabiri, D. G. Holmes and B. P. McGrath, "Control of Active and Reactive Power Ripple to Mitigate Unbalanced Grid Voltages," in *IEEE Trans. Ind. Appl.*, vol. 52, no. 2, pp. 1660-1668, March-April 2016.

[28] Hong-Seok Song and Kwanghee Nam, "Dual current control scheme for PWM converter under unbalanced input voltage conditions," in *IEEE Trans. Ind. Electron.*, vol. 46, no. 5, pp. 953-959, Oct 1999.

[29] K. Jia, Z. Ren, L. Li, Z. Xuan and D. Thomas, "High-frequency transient comparison based fault location in distribution systems with DGs," in *IET Generation, Transmission & Distribution*, vol. 11, no. 16, pp. 4068-4077, 11 9 2017.

[30] D. Pan, X. Ruan, C. Bao, W. Li and X. Wang, "Capacitor-Current-Feedback Active Damping With Reduced Computation Delay for Improving Robustness of LCL-Type Grid-Connected Inverter," in *IEEE Trans. Power Electron.*, vol. 29, no. 7, pp. 3414-3427, July 2014.

[31] D. Yang, X. Ruan and H. Wu, "Impedance Shaping of the Grid-Connected Inverter with LCL Filter to Improve Its Adaptability to the Weak Grid Condition," in *IEEE Trans Power Electron.*, vol. 29, no. 11, pp. 5795-5805, Nov. 2014.

[32] S. Liu, T. Bi, K. Jia and Q. Yang, "Coordinated fault-ride-through strategy for doubly-fed induction generators with enhanced reactive

and active power support," in *IET Renewable Power Generation*, vol. 10, no. 2, pp. 203-211, 2 2016.

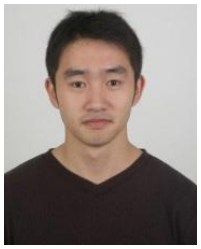

Ke Jia was born in China in 1986. He received his M.Sc and Ph.D. degree in electrical engineering from Nottingham University, U.K., in 2008 and 2011, respectively and then worked as a Research Fellow until 2013.

He is currently an Associate Professor at North China Electric Power University. His research interests include power system protection and fault location, microgrid automation and renewable energy.

Zhe Yang was born in China in 1994. He received the bachelor's degree in electrical engineering from the Northeast Electric Power University in 2017.

He is currently pursuing the master's degree in electrical engineering with North China Electric Power University. His research interests include analysis of power system with renewable energy, power system protection and control.

Yu Fang received the B.Eng. degree in electrical engineering from the Department of Electrical Engineering in North China Electric Power University, Beijing, China, in 2017, where he is currently pursuing the M.Eng. degree in electrical engineering.

His current research interests include analysis of power system with renewable energy, power system protection and control.

Tianshu Bi (M'98, SM'09) received the Ph.D. degree from the Department of EEE in the University of Hong Kong in 2002.

She is currently a professor at North China Electric Power University. Her research interests include power system protection and control, synchronized phasor measurement technique and its application.

Mark Sumner (SM'05) received the B.Eng degree in Electrical and Electronic Engineering from Leeds University in 1986 and then worked for Rolls Royce Ltd in Ansty, UK. Moving to the University of Nottingham, he completed his PhD in induction motor drives in 1990, and after working as a research assistant, was appointed Lecturer in October 1992.

He is now Professor of Electrical Energy Systems. His research interests cover control of power electronic systems including sensorless motor drives, diagnostics and prognostics for drive systems, power electronics for enhanced power quality and novel power system fault location strategies.